

Nitrogen doped In₂O₃-ZnO nanocomposite thin film based sensitive and selective ethanol sensor

P. K. Shihabudeen¹ and Ayan Roy Chaudhuri^{1}*

¹ *Materials Science Centre, Indian Institute of Technology Kharagpur, 721302 Kharagpur, West Bengal, India*

Abstract

Nanocomposite metal oxide thin films exhibit assuring qualities in the field of gas sensors because of the collective opportunities provided by the heterointerface formation. In this work, we present the synthesis of nitrogen doped mesoporous In₂O₃-ZnO nano-composite thin films by simple wet chemical method using urea as the nitrogen precursor. SEM investigation suggests formation of mesoporous nano-composite thin films, where the uniformity of surface pore distribution depends on the relative proportion of In₂O₃ and ZnO in the composites. HRTEM investigation suggest formation of sharp interfaces between N-In₂O₃ and N-ZnO grains in the nano-composite thin films. The nano-composite thin films have been tested for their ethanol sensing performance over an extensive range of temperature, ethanol vapor concentration and relative humidity. Nitrogen doped nano-composite thin film with equal proportion of In₂O₃ and ZnO exhibits excellent ethanol sensing performance at a reasonable operating temperature (~94 % at 200 °C for 50 ppm of ethanol), fast response time (~two seconds), stability over time, enhanced resilience against humidity and selectivity to ethanol over various other volatile organic compounds. All the

* Corresponding author: Tel: +91-3222-283978

Electronic mail: ayan@matsc.iitkgp.ac.in (Ayan Roy Chaudhuri)

results indicated that nitrogen doped $\text{In}_2\text{O}_3/\text{ZnO}$ nano-composite thin film portrays great possibilities in designing improved performance ethanol sensor.

Keywords: Zinc oxide, Indium oxide, heterostructure, ethanol detection

1. Introduction

Ethanol is a volatile organic compound (VOC) commonly used in industrial as well as domestic applications ^{1,2}. Increased utilization of ethanol in industry rises the danger of explosion as well as ground-water contamination ^{3,4}. Moreover, the leading source for road accidents around the world is due to driving under the influence of alcohol. In addition, metabolically generated ethanol in breath also acts as biomarker related to liver diseases such as cirrhosis and fatty liver ⁵. Semiconducting metal oxide (SMO) based thin film gas sensor is a promising candidate to monitor VOCs offers advantages like chemical stability, good sensitivity, detection of wide range of gases etc. ^{6,7}. Despite their promising sensing performance toward VOCs the SMO based gas sensors suffer from drawbacks such as high operating temperature, slow sensing and cross-sensitivity ^{8,9}. In order to circumvent the issues, numerous approaches have been utilized like surface microstructure modification, multiple metal oxide nanocomposite thin films, composites with noble metals, dopant incorporation etc ^{10,11}.

Among these approaches oxide nanocomposites and incorporation of suitable dopants in oxides offers distinct advantages. Fabrication of nanocomposite thin films significantly enhances the sensing characteristics due to their varying compositions and the synergistic effects (geometrical effects, chemical effects and electronic effects) in the composites ^{12,13}. The nanoscale heterojunctions in the composite thin films modify the

electronic structure and increases the oxygen vacancy concentration, which in turn affect the selectivity and sensitivity towards gases ^{14,15}. In₂O₃ and ZnO are two common SMOs which have been extensively studied for gas sensing. The composites and heterostructure of these two oxides in form of like microsphere ¹⁶, nanosheet ¹⁵, nanofiber ¹⁷ and nanowire ¹⁸ are reported for ethanol sensing application. Even though the hetero structures have displayed superior ethanol sensing performance compared to the individual oxides, they still suffer from high operating temperature, slow response time and cross-sensitivity ^{14,19}. Additionally, the complex nanostructures often suffer from temporal and thermal instabilities. In this context thin film-based sensors are considered as suitable alternative to overcome the shortcomings of nanostructures ²⁰.

In contrast, doping induces changes in electronic structure, chemical bonding and oxygen vacancy concentration which leads to selective adsorption of gas molecules ^{21,22}. In our previous reports on nitrogen doped In₂O₃ and ZnO thin films, an improved performance on ethanol sensing characteristics compared to their corresponding pristine oxides has been observed ²². The N-In₂O₃ thin film has displayed a fast and stable response, whereas N-ZnO thin film exhibited selective and low temperature sensing. In both cases changes in band gap and increase in oxygen vacancy has been observed. Based on our observations it appeared that nano composite thin film-based sensors consisting of N-In₂O₃ and N-ZnO shall be an efficient approach of producing fast and selective chemiresistive ethanol sensor.

This work focuses on preparation of nanocomposite thin films of N-In₂O₃/N-ZnO with different concentration of the nitrogen doped oxides in the composite and elucidate their ethanol sensing characteristics. We demonstrate that the nitrogen doped composite thin film with optimum composition exhibit superior sensing response, faster response time, selectivity towards ethanol, and excellent stability over a wide range of relative humidity

condition in comparison to the undoped composite sensor as well as nitrogen doped individual oxides.

2. Experimental

2.1 Thin film synthesis

Urea (Alfa-aeser, >99 %), Zinc acetate dihydrate (Merk, >99%) and Indium acetate (Alfa-aeser, >99%) were used as precursor for nitrogen, zinc and indium respectively for the thin film synthesis. At first, the sol has been synthesised, for which a solution of zinc acetate and indium acetate was prepared in 10 ml of ethanol (99.9 %) as shown in table S1. Ethanolamine (3ml), was added drop wise to the solution while stirring at 60 °C. Urea (1.2 g) was dissolved in 10 ml of ethanol in a separate beaker at similar stirring conditions. Thereafter, these two solutions were mixed together and it was stirred at 60 °C for 4 hours till a stable reddish-orange solution was obtained²². Thin films have been prepared by spin coating of the sol at 3000 rpm for 20 seconds on pre-cleaned SiO₂/Si substrates. After coating, the solvents were removed by drying it on a hot plate at 125 °C. The composite film with similar thickness was prepared by coating the sol multiple times. Finally the samples have been annealed at 750 °C for one hour to obtain crystalline thin films. Samples were named IZON 25, IZON 50 and IZON 75 which has 25 %, 50 % and 75 % In₂O₃ in the composition respectively. Similarly, a reference sample IZO 50 without urea was synthesised following above-mentioned procedure.

2.2 Material characterisation

Panalytical Empyrion X-ray diffraction (XRD) Machine with a Cu K- α radiation source (1.54 Å) was used to determine the crystal structure of the synthesised thin films. Field emission scanning electron microscope (FESEM Zeiss Gemini, Germany) was used to analyse the surface microstructure and cross-section of the samples. The transmission electron microscopy analysis was performed using FEI TECNAI G2 F20 X-TWIN. X-ray photoelectron spectroscopy (model PHI 5000 Versa Probe II, INC, Japan) with Al K- α x-ray source (1486.6 eV) was used to study the surface chemical composition.

2.3 Sensor measurements

Gold was used as the electrodes for ethanol sensing characteristics. An interdigitated electrode with 2 mm width and 1.5 mm electrode separation was sputtered on to the thin films. An inhouse built quasi-static gas sensing setup was used to carry out the VOC sensing measurement. A load resistance (R_L), which has a similar resistance of the sensing film is connected in series and a continuous ~5 V DC is supplied over the sensor. A data collecting arrangement based on a microcontroller (Atmel ATMEGA 32) is employed to measure the net output voltage across R_L . For additional evaluation and data storage, the whole setup is connected to a desktop computer via the RS232 interface. The detailed measurement process could be found in our previous work²². The sensor response (S) of the thin films were calculated using the following relation

$$S(\%) = \frac{(R_a - R_g)}{R_a} \times 100 \quad (1)$$

Where R_g and R_a are the equilibrium resistances measured in the presence of test gas and air, respectively. The response (τ_{res}) and recovery (τ_{rec}) time were estimated as the time taken to

raise base resistance to 90% of the maximum resistance and the time taken for resistance to fall 90% of the equilibrium resistance in the air.

3. Material characterization

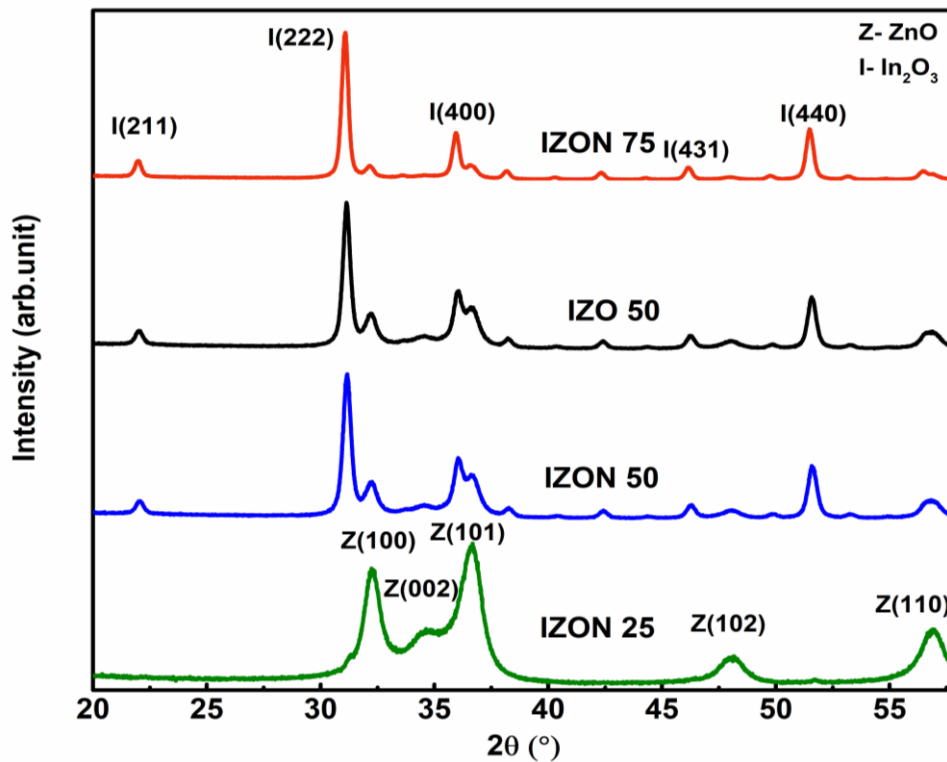


Figure 1. XRD of various composite thin films.

Figure 1 portrays the XRD patterns of different composite thin films. The diffraction peaks have been marked in accordance to typical diffraction pattern for cubic In_2O_3 (JCPDS 006-0416) and wurtzite ZnO (JCPDS 36-1451). All the films are well crystalline which exhibit diffraction peaks corresponding to both In_2O_3 and ZnO . While ZnO rich (75%) IZON 25 has shown intense peaks which correspond to ZnO (100),(002) and (101) planes, with increase of In_2O_3 fraction, intensity of the In_2O_3 peaks increase. No obvious shift has been observed with nitrogen doping for composite films of similar composition, e.g. IZON 50

and IZO 50. On the other hand a slight shift in peaks has been observed with variation in film composition (figure S1).

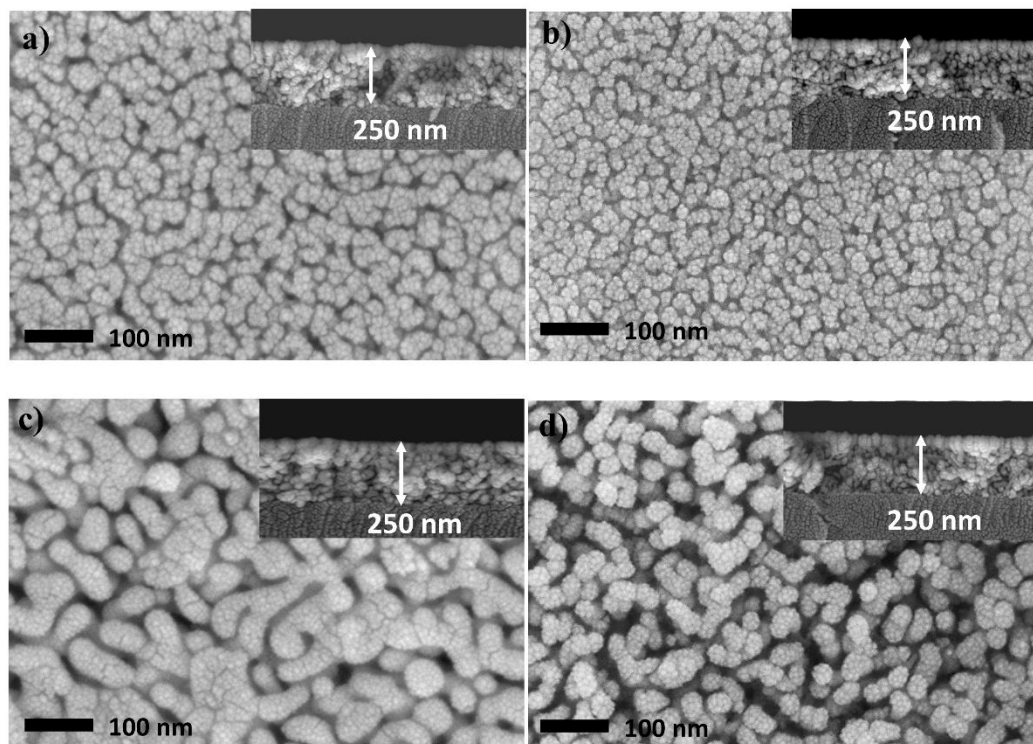


Figure 2. scanning electron microscopy images of a) IZON 25, b) IZON 50, c) IZON 75 and d) IZO 50 composite thin films (cross-sectional SEM in the inset).

Scanning electron microscopy has been carried out to investigate the surface microstructure of composite thin films. Figure 2 depicts the SEM surface images of the thin films. All the films exhibit mesoporous surface morphology. The pore size distribution in the composite thin films has been estimated from the SEM image analysis (figure S2). While the IZON 50 thin film possesses an average pore diameter of ~ 24 nm, the IZO 50 film has larger pores with average diameter of ~ 52 nm. IZON 25 thin film has been found to possess pore size (~ 26 nm) similar to that of IZON 50, but with larger agglomerated grains. On the other hand, IZON 75 formed larger pores (~ 41 nm) and agglomerated

particles. Large amount of In_2O_3 in IZON 75 and ZnO in IZON 25 leads to an agglomerated structure and reduces surface pore distribution on the the film ²³. The surface pore coverage for the composite thin films has been estimated from the post image analysis using ImageJ software of corresponding SEM images (figure S3). The estimated values are 30%, 40 %, 22 % and 26 % for IZON 25, IZON 50, IZON 75 and IZO 50 thin films respectively. All the samples have comparable thickness of ~ 250 nm as observed from the cross-sectional SEM images (inset, figure 2).

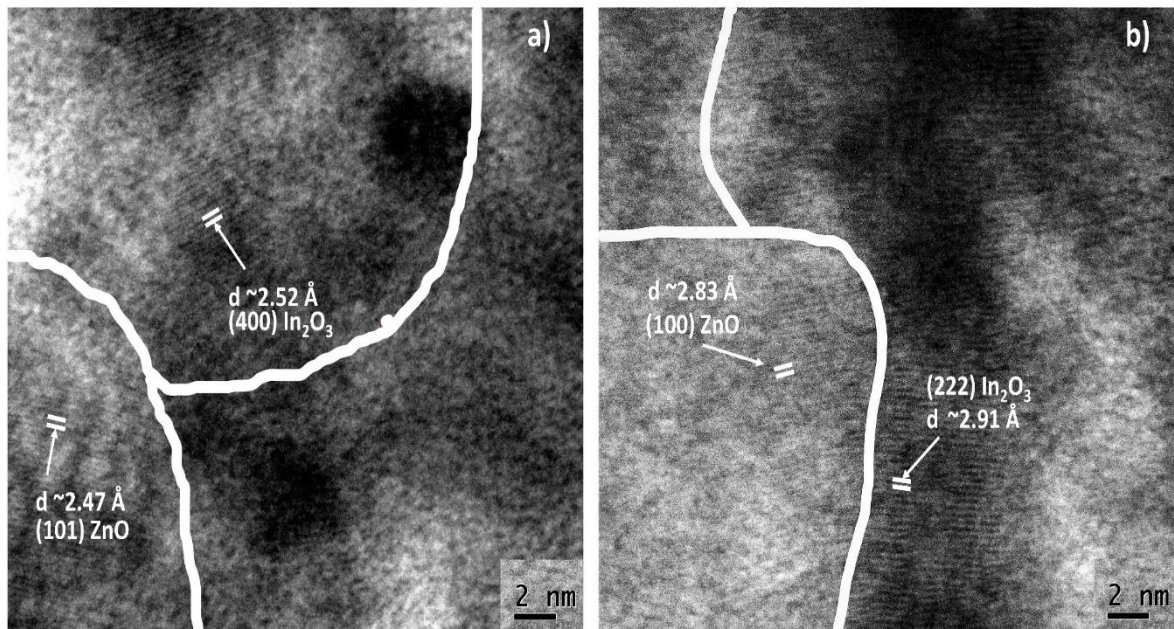


Figure 3. TEM images of a) IZON 50, b) IZO 50 composite thin films.

In order to confirm the formation of heterojunction between the two oxides in the nanocomposite thin films, the samples have been investigated by transmission electron microscopy (TEM). Figure 3 displays TEM images of IZO 50 and IZON 50 as representative samples. The TEM images confirm high crystallinity of cubic In_2O_3 and hexagonal ZnO. In both the composite thin films formation of nano-scale heterojunction without any detectable

intermixing has been confirmed from figure 3(a-b), which display two distinct regions (marked with white lines) with d spacing values corresponding to cubic In_2O_3 crystal structures and wurtzite ZnO. Creation of well-constructed heterojunction between ZnO and In_2O_3 with good crystallinity is important for the efficient interfacial charge carrier separation or transportation²⁴.

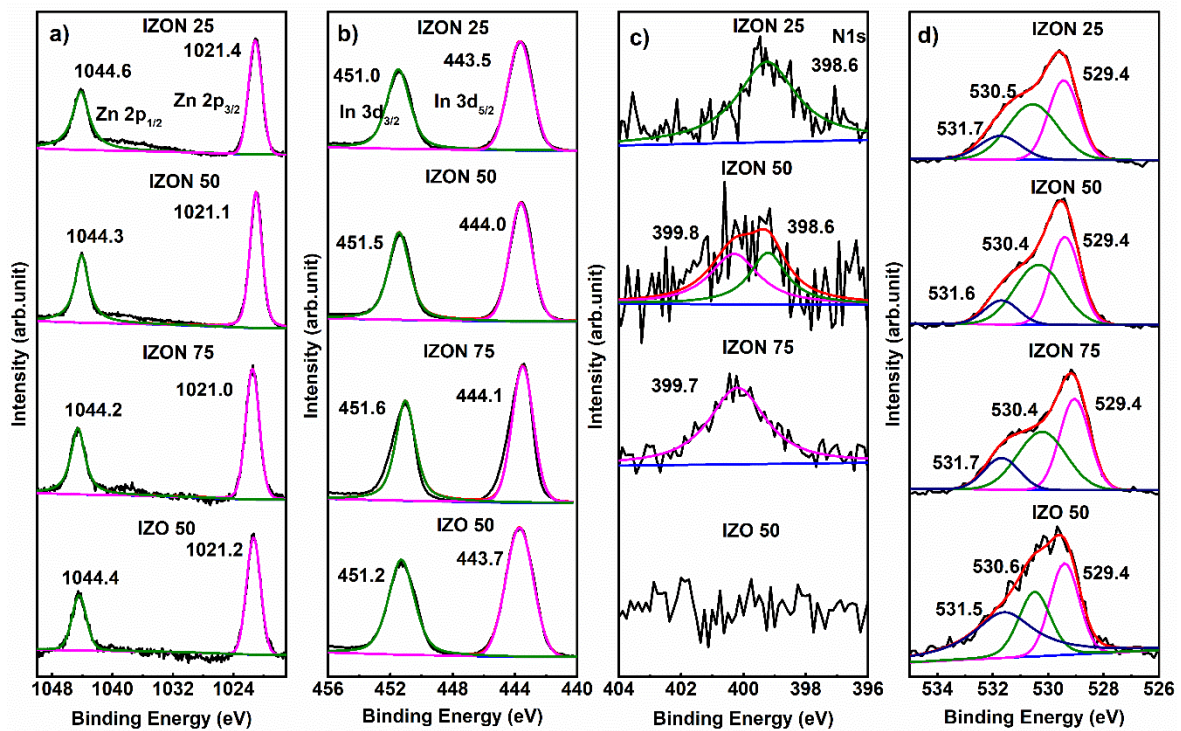


Figure 4. High resolution XPS spectrum of a) Zn 2p, b) In 3d, c) N 1s and d) O 1s of various composite thin films.

XPS analyses have been performed to evaluate the chemical composition and to confirm nitrogen doping in the composite thin films. Carbon 1 s peak (284.5 eV) has been used as a reference for calibration and Tougaar background have been used for the peak background correction²⁵. Figure 4 (a) and 4(b) display the Zn 3p and In 3d peaks of the composite thin films. The doublet peaks of In 3d and Zn 2p have been attributed to In^{3+} and

Zn²⁺ states respectively¹⁶. In 3d peaks exhibit a rigid shift to higher binding energy with increase in In₂O₃ composition in the composites, whereas, the Zn 2p peaks shifted to lower binding energy. The opposite shift of In³⁺ and Zn²⁺ peaks has been attributed to transfer of electrons from low work function In₂O₃ to high work function ZnO across the nanoscale heterojunctions in the composites^{24,26}. The difference in the binding energy positions of the In³⁺ and Zn²⁺ peaks in IZO50 and IZON50 can be attributed to the increase in n-type characteristics due to nitrogen doping^{22,25}. In:Zn ratio for each composite films has been estimated as 28:72, 51:49, 76:24 and 51:49 for IZON 25, IZON 50, IZON 75 and IZO 50 respectively. The composition of various composite films has been shown in table S2.

Figure 4(c) depicts the high-resolution XPS spectra of the N1s region (396-404 eV) for the composite thin films. While the undoped IZO 50 film does not exhibit any identifiable peak in this region, IZON 50 exhibits a broad peak, which has been deconvoluted into two peaks around 398.6 eV and 399.8 eV. The lower energy peak has been attributed to substitutional(N_s) doping of N in ZnO and the other peak has been identified as interstitial(N_i) doping of N in In₂O₃ in agreement to the previous literature reports^{22,27}. The ratio of N_i:N_s has been estimated^{22,27} to be 52:48 which is comparable to the estimated In:Zn ratio in the IZON 50 composite thin film. In case of IZON 25 and IZON 75, single N1s peaks have been observed around 398.6 eV and 399.7 eV respectively which correspond to N_s in ZnO and N_i in In₂O₃ respectively²². Due to lower concentration of N-In₂O₃ in IZON 25 and N-ZnO in IZON75 their corresponding N 1S peaks (i.e. N_i and N_s respectively) could not be resolved. However, since all the samples have been prepared under identical conditions, it is envisaged that the N_i:N_s would be similar to the In:Zn ratio in all the composite thin films. The nitrogen concentration for all the N-incorporated composite thin films has been estimated to be ~0.6 at%.

Figure 4(d) represents the O 1s spectra of composite films. For all the films, the O1s peak has been deconvoluted into three peaks corresponding to Metal-Oxygen (~529.4 eV), non-stoichiometric oxygen (~530.4 eV–530.6 eV) and surface adsorbed hydroxyl species (~531.5 eV–531.7 eV) ^{16,28}. The peak corresponding to adsorbed surface hydroxyl has been more pronounced for IZO 50 film compared to the IZON films, which is attributed to reduced adsorption of water molecules on the nitrogen doped metal oxides ^{29,30}. The ratios of areas under curves A_V/A_L (A_V and A_L are the area under the curve for non-stoichiometric and lattice oxygen respectively) for IZON 25, IZON 50, IZON 75 and IZO 50 have been estimated to be 1.12, 1.17, 1.08 and 0.85 respectively. The increase in oxygen vacancy (related to non-stoichiometric oxygen) in the IZON films have been accredited to doping ³¹.

4. Ethanol sensing characteristics

Figure 5(a) compares the temperature-dependent sensing responses (%) of the IZON thin films with IZO 50 for 50 ppm of ethanol in the temperature range of 150 °C - 300 °C. All the sensing responses have been measured within an average error limit of ± 0.3 %. IZON 25 and IZON 50 exhibited superior ethanol sensing response compared to IZO 50 at operating temperatures below 275 °C, while IZON 75 exhibited inferior response. At operating temperatures below 250 °C, IZON 50 exhibited the best sensing response against ethanol among all the composite thin films. In the present study the optimum working temperature has been chosen to be 200 °C at which IZON 50 exhibited a sensing response of ~ 94%. Figure 5(b) and (c) portray response and recovery transient of the thin film sensors at 200 °C against 50 ppm of ethanol. Response time of the IZON 50 sensor has been found to be the fastest (~2 seconds), which is followed by IZON 25, IZO 50 and IZON 75. The recovery time for all the IZON sensors have been found to be similar (~300 s), whereas

IZO50 exhibited slightly lower recovery time (~ 250 s). Table S3 summarizes the response and recovery time of all the sensors against 50 ppm ethanol measured at 200 °C.

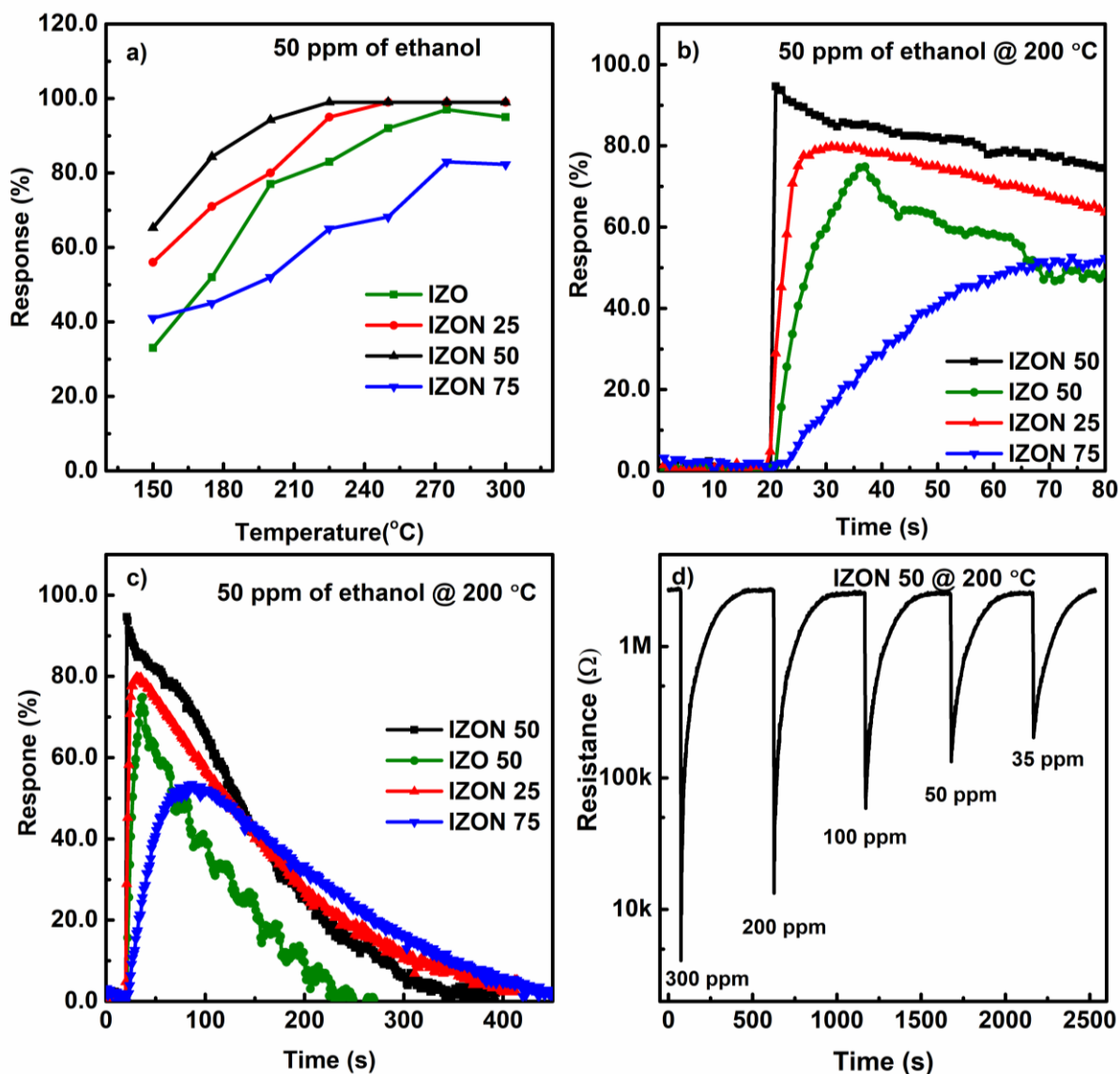


Figure 5 a)) ethanol sensing characteristics of various composite films over a range of temperatures, b) response, c) recovery transient of the various composite thin films 200 °C and d) concentration variation study of IZON 50 thin films at 200 °C.

Based on the superior performance of IZON 50, the sample has been chosen for further investigation. Figure 5(d) depicts the resistance transient of the IZON 50 composite

thin film measured at 200 °C against varied ethanol concentration (35 ppm - 300 ppm). The sensor exhibited significantly higher response of ~99 % against 300 ppm ethanol which has changed to only ~92 % at ethanol concentration as low as 35 ppm.

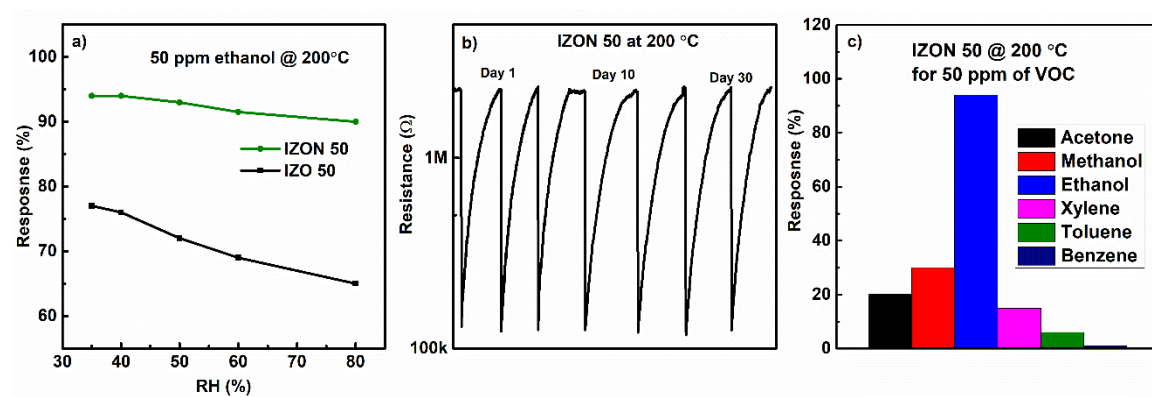


Figure 6 a) stability against relative humidity for both films, b) stability against time for IZON 50 thin film, c) selectivity of IZON 50 film for other VOCs at 200 °C.

Figure 6(a) compares the influence of relative humidity (RH%) on the ethanol sensing properties of IZON 50 and IZO 50. The IZON 50 displays significantly stable response (drop of only 5%) on the other hand the IZO 50 sensor suffers ~15 % reduction in the sensing response over the range of the RH from 10-80%. This observation agrees well with the reported literature that nitrogen incorporation inhibits water adsorption on metal oxides surfaces^{22,30}. Reduced moisture adsorption leads to enhanced adsorption sites for oxygen, which results in higher ethanol sensing response even at high RH conditions³⁰. Ethanol sensing response of IZON 50 has been examined over an extended period. As shown in figure 6(b) good base line recovery together with marginal variation in the sensor response has been attained over a period of one month. Figure 6(c) compares the selectivity of IZON 50 sensor for 50 ppm of ethanol, acetone, methanol, xylene, toluene and benzene measured at 200 °C. The composite film is selective to ethanol compared to other VOCs.

The superior ethanol sensing response of the film agrees well with earlier reported results on the ethanol sensing response of N-ZnO²⁵.

5. Mechanism

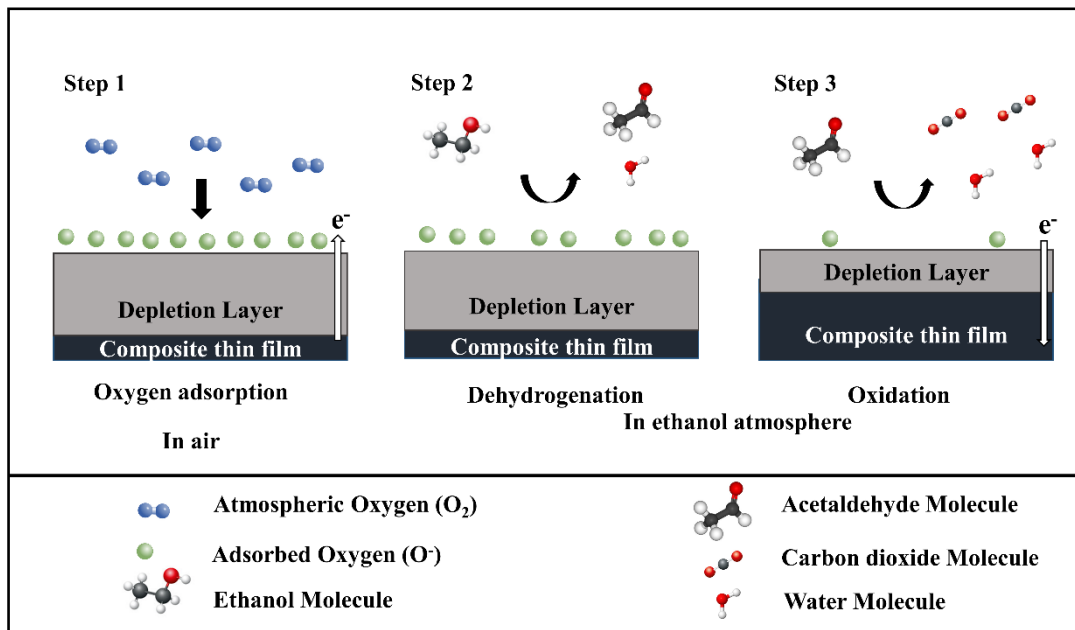


Figure 7 ethanol sensing mechanism of the composite thin film

In order to understand the improved ethanol sensing performance of IZON50, at first the ethanol sensing mechanism is considered. The sensing mechanism of composite thin films has been schematically represented in figure 7. Similar to various n-type chemiresistive oxides, exposing the sensor surface to air leads to adsorption of atmospheric oxygen, which creates surface oxoanions (predominantly O^- species at the sensor operating temperature of 200 °C)³² by capturing electrons from the conduction band of the oxide (step 1). This creates an electron depletion layer at the sensor surface which gives rise to potential barrier between individual grains and increases the overall resistance of the sensor. When the sensor is subjected to ethanol vapour, ethanol molecules get adsorbed on its surface and

get oxidized by the oxoanions (step 2 and step 3) to form carbon dioxide and water according to the reaction,



This releases the electrons back to the conduction band of the oxides, which reduces the depletion layer width and thus the sensor resistance. As we had reported earlier, nitrogen doping increases the V_o concentration in the chosen oxides that leads to an improvement in the dissociative adsorption of atmospheric oxygen on its surface²². Improvement of the receptor function of In_2O_3 (N- In_2O_3) and ZnO (N- ZnO) thin film based sensors because of nitrogen doping leads to their enhanced ethanol sensing performance in comparison to the undoped oxides^{22,25}. Table S4 compares ethanol sensing response and operating temperature of N- In_2O_3 , N- ZnO , IZO50 and IZON50 thin film sensors. Clearly the nitrogen doped nano-composite thin films exhibit superior response compared to the individual oxide thin films. Our observations agree well with the existing literature reports on the significant improvement of reducing gas sensing properties in $\text{In}_2\text{O}_3/\text{ZnO}$ heterojunction based sensors^{15,33}. It is to be noted that the ethanol sensing performance has been significantly enhanced in case of the nitrogen doped nano-composite thin film sensor (IZON50). The improvement of ethanol sensing performance in the nano-composite thin films has been primarily attributed to the formation of the nanoscale heterojunctions between In_2O_3 and ZnO .

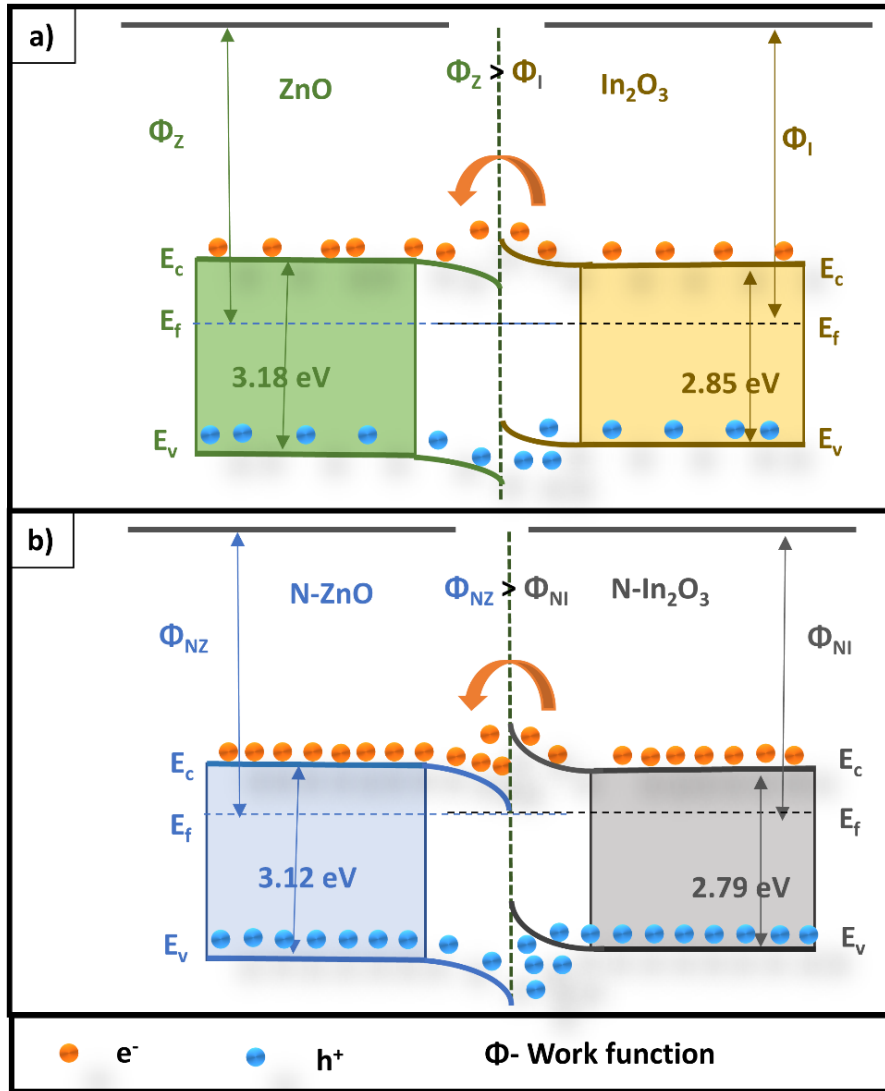


Fig 8. type-II heterojunction formation in a) IZO 50 and b) IZON 50 composite thin films

Formation of nano-scale heterojunctions with sharp interfaces between In_2O_3 and ZnO , and charge transfer from In_2O_3 to ZnO have been confirmed from TEM and XPS analyses respectively. Electron energy band alignment across In_2O_3 and ZnO interfaces has been reported to form type II heterojunction²⁶. Since the work function of ZnO is larger compared to In_2O_3 , transfer of electron occurs from In_2O_3 to ZnO until the Fermi level aligns^{24,34}. The band gaps of ZnO and In_2O_3 thin films have been estimated as 3.18 eV, 2.85 eV respectively from diffuse reflectance spectroscopy study (figure S4) which agree well with

those reported in the literature for oxygen deficient ZnO and In₂O₃^{35,36}. XPS investigation in the valence band region suggests separation between the valence band edge and Fermi level to be ~2.05 eV and ~1.95 eV for In₂O₃ and ZnO thin films respectively (figure S5(a&b)). Figure 8(a) schematically represents the charge transfer across In₂O₃/ZnO interface that leads to the formation of an electron accumulation layer on the ZnO side of the heterojunction. Electron accumulation at the interface gives rise to enhanced reaction sites for the adsorption of oxygen, which results in the improved sensitivity in the In₂O₃/ZnO nanocomposites¹². It has been demonstrated that incorporation of nitrogen in the chosen n-type oxides increases their conductivity due to the enhanced concentration of the V_{OS}^{22,25}. The band gaps of N-ZnO and N-In₂O₃ thin films have been estimate as 3.12 eV and 2.79 eV (figure S4), while the separation between the valence band edge and Fermi level have been 2.2 eV and 2.18 respectively (figure S5(a&b)). This indicates stronger n-type nature of the nitrogen doped oxides compared to the undoped oxides which results in an enhanced electron density at the N-In₂O₃/N-ZnO interface in IZON 50 compared to IZO 50 as depicted schematically in figure 8(b). Enhanced electron concentration at the heterojunction interfaces in IZON 50 provides more reaction sites for oxygen chemisorption that leads to significant improvement in the sensor performance.

Superior performance of IZON 50 compared to the other N-doped nanocomposites is envisaged to be related to their microstructures. As discussed earlier, IZON 25 and IZON 75 possess agglomerated surface morphology, which reduces the active sites for gas adsorption²³. On other hand, IZON 50 possesses mesoporous surface (SEM study) with large number of active sites. Larger surface pore coverage (40 %) in IZON 50 increases the active sites for adsorption. Table 1 compares ethanol sensing characteristics (e.g. response, operating temperature, response time and test gas concentration) of the present IZON50

sensor with those reported for various thin film and nanostructure-based sensors consisting of In₂O₃ and ZnO as the sensing materials. Inspecting the table, it is clear that ethanol sensing characteristics of IZON 50 thin film is superior compared to many of the routinely investigated sensors.

Table 1. Comparison of ethanol sensing characteristics of our study with literature

Sl. No	Sensing Material	Working Temperature (°C)	Concentration (ppm)	Response		Response time(s)
				(%)	Ra/Rg	
1	In-doped 3DOM ZnO ³⁷	250	100	-	88	N/A
2	Pd-ZnO nanorods ³⁸	260	500	-	5.12	56
3	N-In ₂ O ₃ thin film ²²	250	300	-	333	1
4	N-ZnO thin film ²⁵	225	300	-	324	12
5	In ₂ O ₃ /ZnO nanostructure ¹⁴	250	300	-	900	25
6	In ₂ O ₃ /ZnO core-shell nano fiber ¹⁷	225	200	-	57	4
7	In ₂ O ₃ /ZnO nanosheet ¹⁵	240	100	-	300	45
8	N-In ₂ O ₃ /N-ZnO composite thin film (this work)	200	300	~99	324	~2

6. Conclusion

In summary, a robust, highly sensitive, selective, fast and reproducible ethanol sensor has been fabricated by wet chemical synthesis of nitrogen doped $\text{In}_2\text{O}_3/\text{ZnO}$ nanocomposite mesoporous thin films on SiO_2/Si substrates. XPS investigation of the nano-composite thin films indicates nitrogen doping at the interstitial sites of In_2O_3 and substitutional sites of ZnO . TEM investigations confirm sharp interface between the In_2O_3 and ZnO grains indicating successful formation of n-n heterojunction. The uniqueness of the mesoporous nitrogen doped nanocomposite sensor with equal concentration of the oxide components is the availability of uniform pore distribution on the surface of the sensor and n-n heterojunctions with higher electron concentration compared to undoped nano-composite sensor. This leads to significantly higher ethanol sensing response ($\sim 94\%$) and a fast response time ($\sim 2\text{ s}$) at a moderate operating temperature of $\sim 200\text{ }^\circ\text{C}$. The sensor exhibits excellent stability over a long duration and resilient to relative humidity conditions as high as 80%. Further, the sensor is highly selective to ethanol compared to various other volatile organic compounds. The experimental results suggest that incorporation of nitrogen in $\text{In}_2\text{O}_3/\text{ZnO}$ nano-composite thin film is an effective route to improve the adsorption efficiency of ethanol molecules and facilitating the propagation of charge carriers across its surface. The present work presents a strategy to develop efficient ethanol sensor for utilization in law enforcement and biomedical applications both in terms of cost effectiveness and performance.

7. References

- 1 L. Meng, *Ethanol in automotive applications*, Elsevier Inc., 2018.
- 2 G. Dharmalingam, R. Sivasubramaniam and S. Parthiban, *J. Electron. Mater.*, 2020, **49**, 3009–3024.
- 3 J. G. Freitas, B. Fletcher, R. Aravena and J. F. Barker, *Ground Water*, 2010, **48**, 844–857.
- 4 S. E. Powers, C. S. Hunt, S. E. Heermann, H. X. Corseuil, D. Rice and P. J. J. Alvarez, *Crit. Rev. Environ. Sci. Technol.*, 2001, **31**, 79–123.
- 5 M. Righettoni, A. Amann and S. E. Pratsinis, *Biochem. Pharmacol.*, 2015, **18**, 163–171.
- 6 H. Ji, W. Zeng and Y. Li, *Nanoscale*, 2019, **11**, 22664–22684.
- 7 N. Yamazoe and K. Shimano, in *Semiconductor Gas Sensors*, Elsevier, 2013, pp. 3–34.
- 8 K. Inyawilert, A. Wisitsora-At, A. Tuantranont, P. Singjai, S. Phanichphant and C. Liewhiran, *Sensors Actuators, B Chem.*, 2014, **192**, 745–754.
- 9 L. Xu, M. Ge, F. Zhang, H. Huang, Y. Sun and D. He, *J. Mater. Res.*, 2020, **35**, 3079–3090.

- 10 G. F. Fine, L. M. Cavanagh, A. Afonja and R. Binions, *Sensors*, 2010, **10**, 5469–5502.
- 11 A. Mirzaei, S. G. Leonardi and G. Neri, *Ceram. Int.*, 2016, **42**, 15119–15141.
- 12 C. Han, X. Li, Y. Liu, X. Li, C. Shao, J. Ri, J. Ma and Y. Liu, *J. Hazard. Mater.*, 2021, **403**, 124093.
- 13 D. R. Miller, S. A. Akbar and P. A. Morris, *Sensors Actuators, B Chem.*, 2014, **204**, 250–272.
- 14 M. Gholami, A. A. Khodadadi, A. Anaraki Firooz and Y. Mortazavi, *Sensors Actuators, B Chem.*, 2015, **212**, 395–403.
- 15 K. Zhang, S. Qin, P. Tang, Y. Feng and D. Li, *J. Hazard. Mater.*, 2020, **391**, 122191.
- 16 S. Wang, X. Wang, G. Qiao, X. Chen, X. Wang and H. Cui, *Sensors Actuators, B Chem.*, 2021, **341**, 130002.
- 17 B. Huang, Z. Zhang, C. Zhao, L. Cairang, J. Bai, Y. Zhang, X. Mu, J. Du, H. Wang, X. Pan, J. Zhou and E. Xie, *Sensors Actuators, B Chem.*, 2018, **255**, 2248–2257.
- 18 N. Singh, A. Ponzoni, R. K. Gupta, P. S. Lee and E. Comini, *Sensors Actuators, B Chem.*, 2011, **160**, 1346–1351.
- 19 Q. Diao, Y. Yin, W. Jia, X. Xu, Y. Ding, X. Zhang, J. Cao, K. Yang and M. Jiao, *Mater. Res. Express*, 2020, **7**, 115012.

- 20 G. Korotcenkov, *Sensors Actuators, B Chem.*, 2005, **107**, 209–232.
- 21 A. Jayalatha, V. Elavalagan and P. Shankar, *Ceram. Int.*, 2016, **42**, 18289–18295.
- 22 P. K. Shihabudeen and A. Roy Chaudhuri, *Sensors Actuators B Chem.*, 2020, **305**, 127523.
- 23 X. Zou, X. Yan, G. Li, Y. Tian, M. Zhang and L. Liang, *RSC Adv.*, 2017, **7**, 34482–34487.
- 24 A. Das, M. Patra, M. Kumar P, M. Bhagavathiachari and R. G. Nair, *Mater. Chem. Phys.*, 2021, **263**, 124431.
- 25 P. K. Shihabudeen, M. Y. Notash, J. J. Sardroodi and A. R. Chaudhuri, *ArXiv*, 2021, 2112.09889.
- 26 L. Ma, H. Fan, H. Tian, J. Fang and X. Qian, *Sensors Actuators, B Chem.*, 2016, **222**, 508–516.
- 27 W. Wen, J. M. Wu and Y. De Wang, *Sensors Actuators, B Chem.*, 2013, **184**, 78–84.
- 28 J. Liu, L. Zhang, B. Cheng, J. Fan and J. Yu, *J. Hazard. Mater.*, 2021, **413**, 125352.
- 29 N. Tit, W. Othman, A. Shaheen and M. Ali, *Sensors Actuators B Chem.*, 2018, **270**, 167–178.
- 30 R. Shanmugam, A. Thamarachelvan and B. Viswanathan, *RSC Adv.*, 2015, **5**, 60524–

- 60533.
- 31 J. J. Macías-Sánchez, L. Hinojosa-Reyes, A. Caballero-Quintero, W. de la Cruz, E. Ruiz-Ruiz, A. Hernández-Ramírez and J. L. Guzmán-Mar, *Photochem. Photobiol. Sci.*, 2015, **14**, 536–542.
- 32 P. K. Shihabudeen and A. Roy Chaudhuri, *J. Mater. Res.*, 2021, **36**, 1561–1572.
- 33 S. Wang, X. Wang, G. Qiao, X. Chen, X. Wang and H. Cui, *Sensors Actuators, B Chem.*, , DOI:10.1016/j.snb.2021.130002.
- 34 R. Vishnuraj, K. K. Karuppanan, M. Aleem and B. Pullithadathil, *Nanoscale Adv.*, 2020, **2**, 4785–4797.
- 35 L. Gai, L. Ma, H. Jiang, Y. Ma, Y. Tian and H. Liu, *CrystEngComm*, 2012, **14**, 7479–7486.
- 36 J. Wang, Z. Wang, B. Huang, Y. Ma, Y. Liu, X. Qin, X. Zhang and Y. Dai, *ACS Appl. Mater. Interfaces*, 2012, **4**, 4024–4030.
- 37 Z. Wang, Z. Tian, D. Han and F. Gu, *ACS Appl. Mater. Interfaces*, 2016, **8**, 5466–5474.
- 38 P. Cao, Z. Yang, S. T. Navale, S. Han, X. Liu, W. Liu, Y. Lu, F. J. Stadler and D. Zhu, *Sensors Actuators B Chem.*, 2019, **298**, 126850.